Research Article

Jakub Horák*, Anton Nikiforov, František Krčma, Matěj Březina, Zdenka Kozáková, Lukáš Dostál, Michal Kalina, and Lukáš Kalina

Synthesis of Ag and Cu nanoparticles by plasma discharge in inorganic salt solutions

https://doi.org/10.1515/ntrev-2022-0549 received October 17, 2022; accepted April 21, 2023

Abstract: In recent years, nanoparticles have emerged as an important player in a broad range of applications, especially thanks to recent advances in their synthesis. The silver and copper nanoparticles are often used due to their antibacterial and fungicidal activities, and this article presents the results of the nanoparticle synthesis using electrical glow discharge generated directly in a volume of their salt solutions. Therefore, there is no influence of air (i.e. reactive nitrogen species) as it is usual in other commonly used approaches. Nanoparticles were prepared under various experimental conditions, and they were characterized by ultraviolet/visible spectrometry, dynamic light scattering, X-ray photoelectron spectroscopy, and high-resolution scanning electron microscopy. Particles were produced without any surfactant or stabilizing agent, and some of them showed higher resistance against agglomeration during their short-term (days) storage. The nanoparticle formation mechanism was confirmed by the fast camera imaging. Thus, the developed approach can be applied for simple environmentally friendly nanoparticle production for various applications.

Keywords: nanoparticle, plasma discharge, silver nanoparticles, copper nanoparticles, discharge in liquids, virtual cathode in liquid, surface plasmon resonance

Anton Nikiforov: Department of Applied Physics, Ghent University, Saint-Pietersnieuwstraat 41 B4, 9000 Ghent, Belgium

František Krčma, Matěj Březina, Zdenka Kozáková, Michal Kalina, Lukáš Kalina: Faculty of Chemistry, Brno University of Technology, Purkyňova 464/118, 612 00 Brno, Czech Republic

Lukáš Dostál: Faculty of Electrical Engineering and Communication, Brno University of Technology, Technická 3058/10, 616 00 Brno, Czech Republic

1 Introduction

Particles with specific size between 10⁻⁹ and 10⁻⁸ m in diameter are called nanoparticles. Materials of these dimensions have different properties from the bulk material. Such particles have very high specific surface area that is important for many applications, including catalysis [1,2] and medicine [3,4]. Nanoparticle properties are dependent not only on the selected material (pure metal, semiconductor, alloy) but also on the size, shape, and crystallographic parameters. All these properties are strongly dependent on the engineering procedure. Thus, nanoparticles made of the same material can have very different properties [5,6]. Silver nanoparticles are used in many application fields such as photovoltaics (diagnostics sensors, solar cells) [7], conductive applications (conductive inks) [8], or cosmetics [9,10]. Copper nanoparticles can be used in similar applications such as silver nanoparticles [10,11], and a big interest is in their catalytic properties [1,12,13]. There is also a growing interest in the use of silver and copper nanoparticles in health care [14-16]. Such applications require nanoparticles in well-defined shapes and especially, a size distribution uniformity. The smaller the nuclei of Ag, the higher antibacterial activity [17]. Nowadays, the silver nanoparticles are already used for biomedical devices (catheters, joint implants, etc.), for wound and bone healing, and others [3]. Silver nanoparticles contained in these products are continuously releasing a small amount of silver ions to provide a protection against bacteria. However, copper nanoparticles show lower antibacterial efficiency compared to silver nanoparticles [15,18], but their green and cost-effective synthesis leads to their application in agriculture [19].

Nanoparticle preparation can be carried out by two generally different approaches. The first one, physical (called also as top-down), is based on the bulk material breaking down into smaller particles. The most often methods are the evaporation–condensation or the laser ablation, both often in the liquid environment. The second approach is a chemical method (also called as bottom-up), mainly based on the reduction from the metal salt solutions (Ag⁺ and Cu²⁺ to Ag⁰ and

^{*} Corresponding author: Jakub Horák, Faculty of Chemistry, Brno University of Technology, Purkyňova 464/118, 612 00 Brno, Czech Republic, e-mail: xchorakj@vutbr.cz

Cu⁰, respectively) by using various reducing agents (sodium citrate, hydrazine, sodium borohydride, and others) [12,13,15,20].

The main disadvantage of both physical and chemical methods is that prepared nanoparticles tend to agglomerate quickly, and thus, their properties are significantly changed. To prevent this, different stabilizing agents such as *N,N*-dimethylformamide [20], polyvinyl pyrrolidone [12,14,20], and polyethylene glycol [12] are commonly used. Their application leads to the particle growth stabilization (in many cases by their surface coating with a thin organic layer), and thus, particles are prevented from a loss of their unique properties [12–15,17,20]. The application of these additives can be rather risky in case of their use in medicine where their residues can be non-acceptable because of their side effects.

A specific nanoparticle formation process was recently proposed based on the combination of plasmas with liquid environment. Such methods are operating at atmospheric pressure and in the presence of liquid (mainly water solutions) and prevent the formation of bigger particles and agglomerates. Moreover, particles can be covered by thin layer of oxides, OH groups, or carbon-containing layers dependent on the used liquid during the formation or immediately after it. Thus, no additional surfactants are necessary to prevent nanoparticles from their agglomeration [21]. The proposed method is an efficient example of the chemical approach where the precursor solution itself serves as a nanoparticle's material source. Many studies were focused on the liquid surface treatment by various gaseous discharges (mostly various jets) or by microplasmas. These discharges are usually formed between the high-voltage (HV) electrode in the gaseous phase (above liquid) and the surface of the grounded solution [22–26].

The application of arc or laser-induced plasmas directly in the liquid phase are the example of the physical approach for the efficient nanoparticle production without surfactants [27,28]. A special way is also the combination of chemical and physical processes for the nanoparticle formation in the liquid phase. The first tests were performed using the laserinduced plasma applied to colloidal nanoparticle solutions [29] or the arc discharge operation in nanoparticle-stabilizing solutions [30]. Some pilot studies of the pure chemical approach using system-generating plasmas directly in liquids were also completed recently [31]. General novelty of our synthesis approach is the fact that thanks to the plasma generation below the solution surface, the formation of reactive nitrogen species is negligible. Nitrogen is coming only from dissolved air and the used salt, and its total concentration is many orders lower than that of oxygen (from deionized water environment). Thus, only reactive oxygen species, atomic hydrogen, and electrons

can be considered during the nanoparticle formation in our novel system where cathode and anode spaces are separated by barrier with small orifice. Two special cathode constructions [32-35] were used for the discharge generation. Thus, electrochemical processes running at the metallic (platinum) anode do not play a role in the nanoparticle formation process. Whole process is running as single step and cost-effective approach using the DC electrical discharge directly generated in the precursor solution without the addition of any hazardous compounds. The discharge generation directly in liquid phase leads to the formation of nanoparticles with suppressed agglomeration. Whole system can also be easily scalable (e.g. the use of a multielectrode system). All these features are important for the greener nanoparticle production in applicable amounts. Simplicity of the used power supply and the use of common cheap precursors brings additional economic benefits. Argon introduction into the discharge volume leads to the lower initial power needed for a breakdown, and thus, lower initial salt concentrations can be used. This leads to the formation of smaller nanoparticles.

The fast camera movies were used to verify the nanoparticle formation process. The role of argon introduced into the discharge on the nanoparticle generation was also investigated. The silver and copper nanoparticles were prepared under selected discharge parameters from their sulphate and nitrate salts, respectively, and they were characterized by the ultraviolet/visible (UV/Vis) spectrometry, dynamic light scattering (DLS), X-ray photoelectron spectroscopy (XPS), and scanning electron microscopy (SEM). Finally, the Tauc plot [36,37] procedure was applied to calculate the band gap energy of the prepared nanoparticles because their surface was oxidized just after their formation in water solutions.

2 Materials and methods

The novelty of this research is in the use of an experimental device depicted in Figure 1, which was used in this work. In general, it is similar as for the discharge generation in the pin-hole configuration [38], where two chambers (electrode spaces) of the glass apparatus are divided by a Teflon diaphragm with the orifice filled by the working solution. The diaphragm is used to separate the anode part and electrochemical processes taking place at the anode surface from the cathode compartment where nanoparticles are synthesized. No discharge is created at the orifice, only at the tip of the used cathode. The whole glass reactor is constructed with a double wall for water cooling.

Figure 1: Double-batch plasma reactor: 1) HV power supply, 2) grounded cathode, 3) anode, 4) gasket, 5) teflon diaphragm, 6) cooling water inlet, 7) cooling water outlet, 8) anode chamber, and 9) cathode chamber.

Two different grounded cathode configurations were used (Figure 2). Configuration A consists of an electrode head made from Macor ceramics of 10 mm in diameter with a stainless-steel capillary (outer diameter of 1 mm; inner diameter of 0.7 mm). This capillary ends 1 mm before the Macor edge, and thus, a pin-hole is formed in the Macor nozzle [32-34]. Argon at a flow rate of 42 sccm is blown to the electrode tip. Thus, the discharge is generated in argon bubbles containing water vapour coming from the bulk solution. Configuration B is similar, but the stainless-steel capillary is replaced by a tungsten rod of the same diameter (i.e. 1 mm) that also ends 1 mm before the Macor edge [35]. This allows the discharge generation in water vapour bubbles generated by the Joule heating. Details about this special discharge can be found in the previous study [35]. Both discharge configurations were sustained for 3 min by DC voltage of about 1.3 kV corresponding to 50 W supplied power.

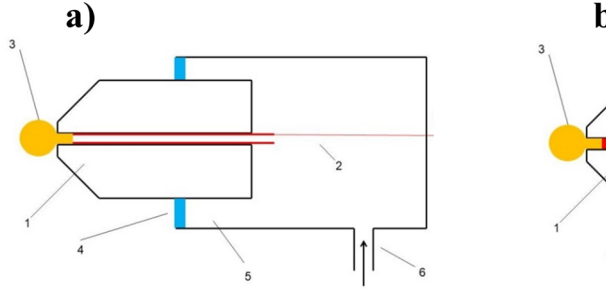
A planar platinum anode (the active area in the liquid of $15 \times 25 \,\mathrm{mm^2}$) connected to the HV source was used for both copper and silver nanoparticle preparation. Copper

nanoparticles were synthetized in the working solution of copper sulphate (CuSO₄) as a precursor. The initial concentrations of 25, 50, 75, and 100 mg/l were tested. Silver nanoparticles were synthesized in the working solution of silver nitrate (AgNO₃) with initial concentrations of 1, 10, 25, 50, and 100 mg/l. To prepare our working solutions, deionized water with conductivity adjusted by appropriate electrolyte was used. Stock solution of NaNO₃ (or Na₂SO₄, respectively) in deionized water was prepared with a conductivity of 950 µS/cm (the concentration of such solution was 560 mg/l NaNO₃ and 460 mg/l Na₂SO₄). This stock solution was used instead of pure deionized water to dissolve the precursor salts, which increased its final conductivity by about 50 μS/cm.

The conductivity adjustment was performed to lower the DC voltage needed for plasma generation and to maintain the stability of the discharge as was also done in the previous study [39] with one-chamber reactor. Solutions were mixed by self-mixing as shown in the supplementary movies presented in the study by Krčma et al. [35].

The nanoparticle formation process was observed by ultrafast camera movies using the Photron FASTCAM SA-X2 perpendicularly to the cathode axis. An additional cubic polycarbonate vessel with a quartz window of 50 mm in diameter was used for this purpose. The discharge vessel was illuminated by two Dedolight halogen lamps Dedocool installed perpendicularly one to the other and to the optical axis. The frame exposure time of 80 µs at 10,000 frames per second and the full chip image were used. The discharge time evolution was visualized with the high space resolution of 50 microns per pixel.

The prepared colloid solutions of nanoparticles were characterized by UV/Vis spectrometer Helios Omega (ThermoFisher Scientific). Obtained absorption spectra for copper nanoparticles were used to calculate the direct band gap energy using the Tauc plot method. This gives relation $(\alpha h \nu)^2$ to the photon energy (α is the absorbance, h is the Planck constant, and ν is the radiation frequency). Morphology, size, and surface



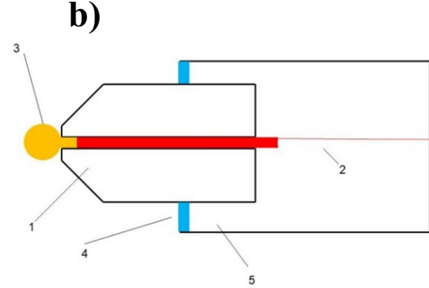


Figure 2: Schemes of cathode configurations: 1) Macor body, 2) stainless-steel capillary a) or tungsten wire b), 3) plasma in bubble in liquid, 4) silicone glue, 5) glass tube, and 6) gas inlet.

topography of nanoparticles were studied by the DLS (Zetasizer Nano ZS, Malvern Panalytical), XPS (Kratos AXIS ULTRA DLD), and the high-resolution scanning electron microscope JEOL JSM-7600F. XPS analyses were carried out with Axis Ultra DLD spectrometer using a monochromatic Al K α ($h\nu$ = 1486.7 eV) X-ray source operating at 75 W (5 mA, 15 kV). The spectra were obtained using an analysis area of ~300 × 700 μ m. The high-resolution spectra were measured with the step size of 0.1 and a pass energy of 20 eV. Instrument base pressure during the measurements was constant at 2 × 10⁻⁸ Pa. Spectra were analysed using CasaXPS software (version 2.3.15) and have been charge-corrected to the main line of the carbon C 1s spectral component (C–C, C–H) set to 284.8 eV. A standard Shirley background was used for all sample spectra.

3 Results and discussion

The bubble formation occurs independently on the used cathode configuration (with [33] or without [35] argon flow). In case of the discharge without argon flow, the bubble is created due to the extensive Joule heating localized close to the cathode tip. In case of the configuration with argon flow, there are two mechanisms coupled to each other – bubble is formed not only due to the argon flow, but also due to the Joule heating like in the previous case. The discharge starts to propagate inside the bubble, *i.e.* in the gaseous phase (in pure water vapour or in argon with saturated water vapour, respectively). The bubble is enlarged in both cases up to the point where the bubble collapses and the discharge is switched off. Then, the process repeats again, so the discharge operation is self-pulsing as confirmed by the current–voltage records. Examples of

typical current–voltage waveforms are presented in Figure 3. The period of the discharge on is about 100 μ s. In case of the operation without argon, there is one current peak seen per each period. But if the system is operating with argon, the secondary peak can be seen after the primary peak, *i.e.* when the bubble collapses. We suppose that there are some ions remaining in the electrode vicinity that can initiate an additional smaller discharge, which is not significant due to insufficient power output. This secondary discharge is observed with a typical delay of about 50 μ s. Additionally, the frequency of the discharge self-pulsing is higher in the case when argon is used.

Due to the two-chamber system, we observed an effect of ion separation due to electrolysis – no such thing can be seen in case of common jet treatments in one-chamber setups [31,39,40]. We observed similar trends as in the previously published study [41], where the pin-hole system in the diaphragm configuration was used. While conductivity slightly rose in both cathode and anode parts, we observed strong difference in pH values. For Ag nanoparticles prepared in 50 mg/l solution, an increase of pH in the cathodic part from pH 5.5 to pH 10.7 (with Ar) or pH 10.1 (without Ar) was found, while it dropped to pH 2.6 (with Ar) or pH 2.4 (without Ar) in the anode part. In case of solution of Cu nanoparticles prepared from 75 mg/l solution, the change from pH 5.3 to pH 6.3 (with Ar) or pH 7.0 (without Ar) and a decrease to pH 2.6 (Ar) or pH 2.6 (without Ar) in the anode part was determined. The difference in the pH increase in the cathodic parts for Cu and Ag is very probably caused by their different ionic mobility. On the other hand, acidic pH in the anodic part was caused by higher H⁺ ion mobility. The higher pH value for Ag nanoparticles not only corresponds with the previous findings, but it can also support increased Ag nanoparticle formation (as was also published in the previous studies [42,43]). For Cu nanoparticles, pH

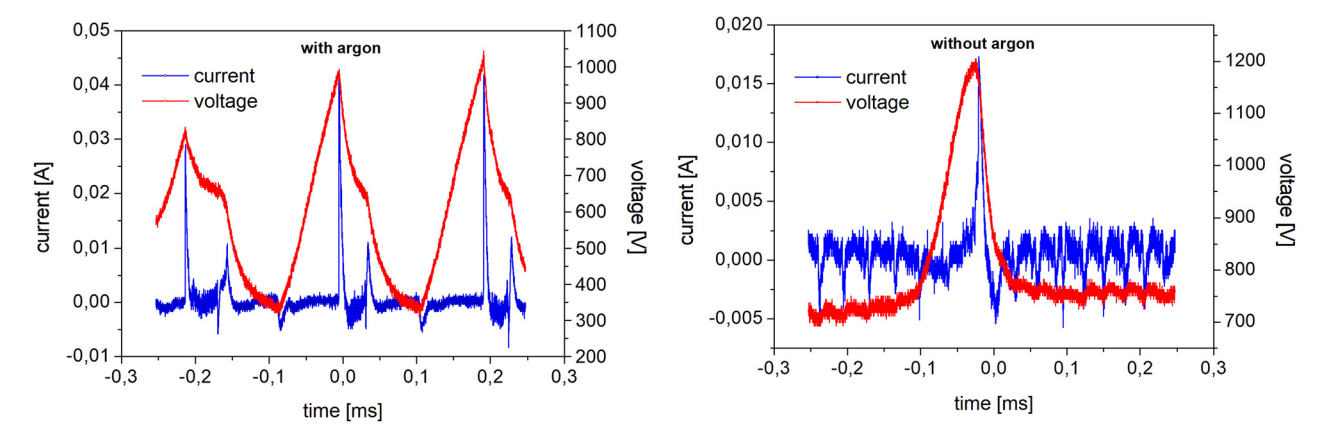


Figure 3: Current-voltage waveforms for the system with and without argon flow.

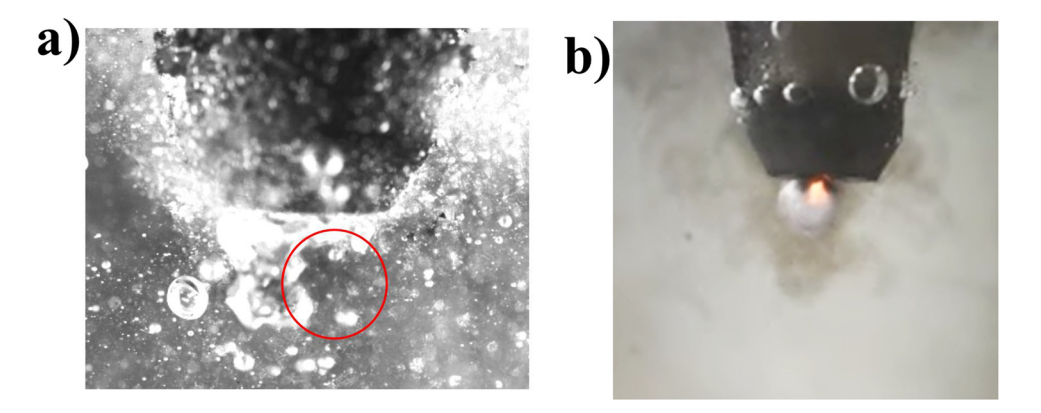


Figure 4: a) Nanoparticles (in the red circle) dissolved into the bulk liquid after the discharge bubble cavitation; b) nanoparticles in the bulk liquid after 5 s of the discharge operation. To see the whole process in the real time, the movie is provided in the supplement.

plays an important role in the control of particle size (e.g. in ref. [44]). Investigation of the pH effect on prepared nanoparticles and their properties will be a part of our next work.

Thus, the plasma is observed between the point cathode and the virtual anode formed by the expanding bubble surface (for its visualization, see in ref. [35]). Metallic cations from the dissociated precursor in liquid are attracted to the bubble surface that plays a role of virtual cathode where solid material is deposited. The process of this deposition takes place only during a very short time period when the discharge is on, and thus, nanoparticles are formed. The short process duration limits the nucleation time and results in the formation of small nanoparticles with the size of tens of nm. When the bubble cavitates, the formed nanoparticles are spread into the bulk liquid and disappear from the electrode vicinity due to the liquid self-mixing. The whole process is well visible on the movie shown in supplementary materials; two selected pictures from the supplementary materials are shown in Figure 4. The process is repeating with the discharge self-oscillation. Schematics of the whole process are shown in Figure 5.

3.1 Synthesis of silver nanoparticles

In the current experiments, we decided to use conductivity adjustments in order to keep the discharge operation stable [35]. The 3 min treated solutions were analysed immediately by the UV/Vis spectrometry. The samples were taken out from the cathode part only, because no nanoparticle production was observed in the anode part of the reactor except negligible diffusion through the separating orifice. The absorption spectra (Figure 6) of the system with or without the argon flow show the main absorption peak at the wavelength of about 425 nm, which indicates the presence of silver nanoparticles. The peak position varies between approximately 413 and 450 nm, which was caused by the surface plasmon resonance effect. This is also well visible by the naked eye as it is shown in Figure 7. Other corresponding pictures can be found in the supplementary materials.

The DLS analysis (three independent replications) showed that the particle size of prepared Ag nanoparticles is rather consistent with exception of the lowest (without Ar) and the

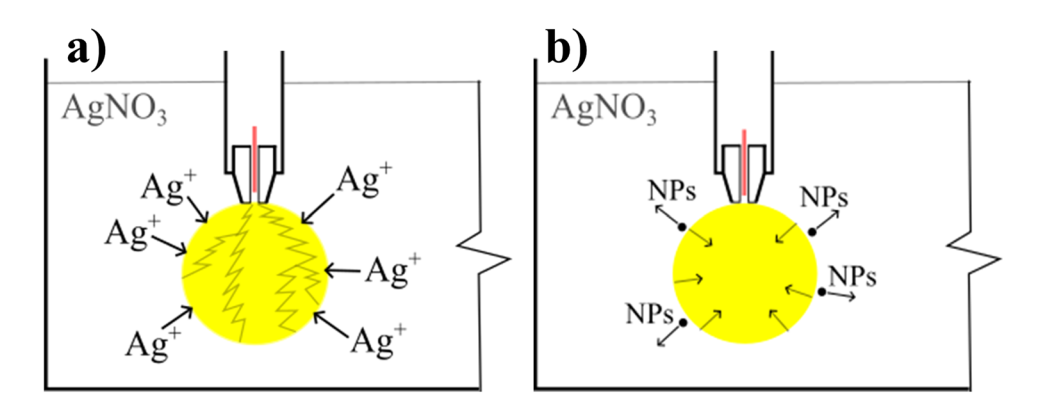


Figure 5: Schematics of the nanoparticle synthesis process: a) metal ions are attracted to the edge of the virtual cathode; b) the bubble cavitates and synthetized nanoparticles are spread into the bulk liquid due to self-mixing.

6 — Jakub Horák *et al.* DE GRUYTER

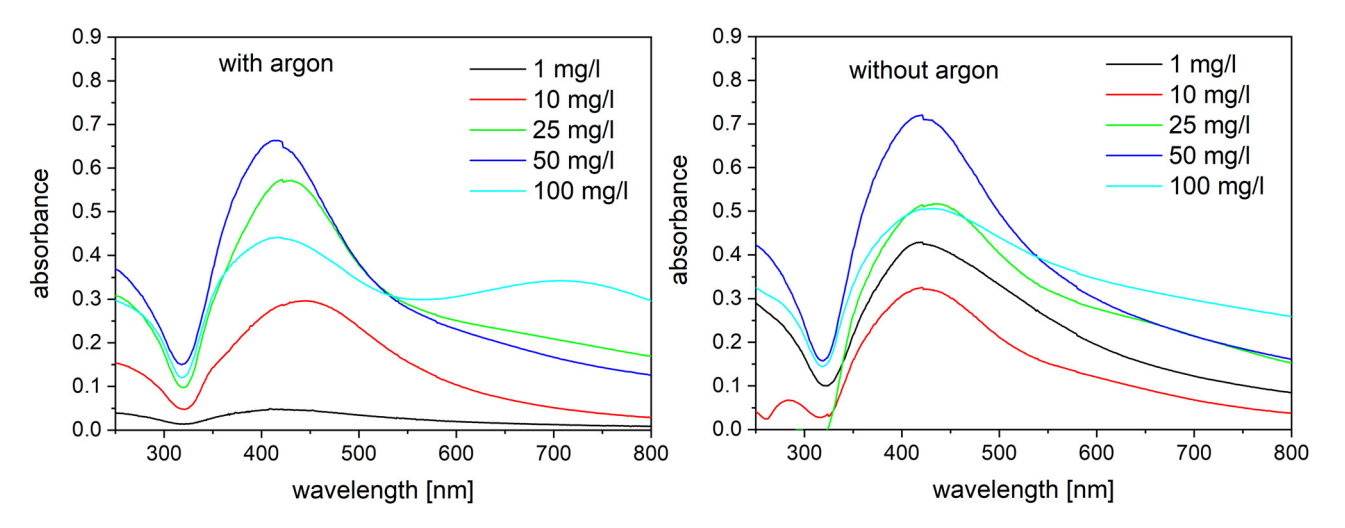


Figure 6: Absorption spectra of the treated silver solutions with and without argon flow.

highest (with Ar) concentrations of AgNO₃ (Table 1 and Figure 8). Overall, DLS shows an interesting concentration effect on nanoparticle size – the higher the salt concentration, the bigger the particle size (Figure 8). These results were confirmed by the SEM analysis as it is shown in Figure 9. Silver formed the spherical-like shaped particles with the size varying in the range of 10–80 nm and agglomerates as observed by SEM images. This could be the effect of the drying process during the preparation.

The XPS surface analysis was performed on selected samples. Results for Ag nanoparticles are presented in Figure 10 where the signal corresponding to the oxidic state of silver as well as a residual signal from the used inorganic salt was detected. The presence of oxygen in the silver nanoparticles was not observed in SEM by EDS as significantly as in the case of Cu nanoparticles, and therefore, we assume mainly the surface oxidation, as confirmed

Table 1: Average diameter results of the DLS analysis for the prepared Ag nanoparticles

		Concentration (mg/l)				
		1	10	25	50	100
Average diameter (nm)	Ar NoAr	48 ± 11 186 ± 8				145 ± 6 59 ± 1

by XPS. Together with plasmonic band in the Ag UV/Vis spectra, these findings suggest that Ag nanoparticles very probably exhibit a core–shell character (Ag/Ag₂O) because the XPS technique is sensitive up to about 5 nm, only, so only a thin surface contributes to the signal. The UV/Vis measurement is not surface-sensitive, only, so the inner part of nanoparticles contributes, too. And the inner part is in the metallic form.

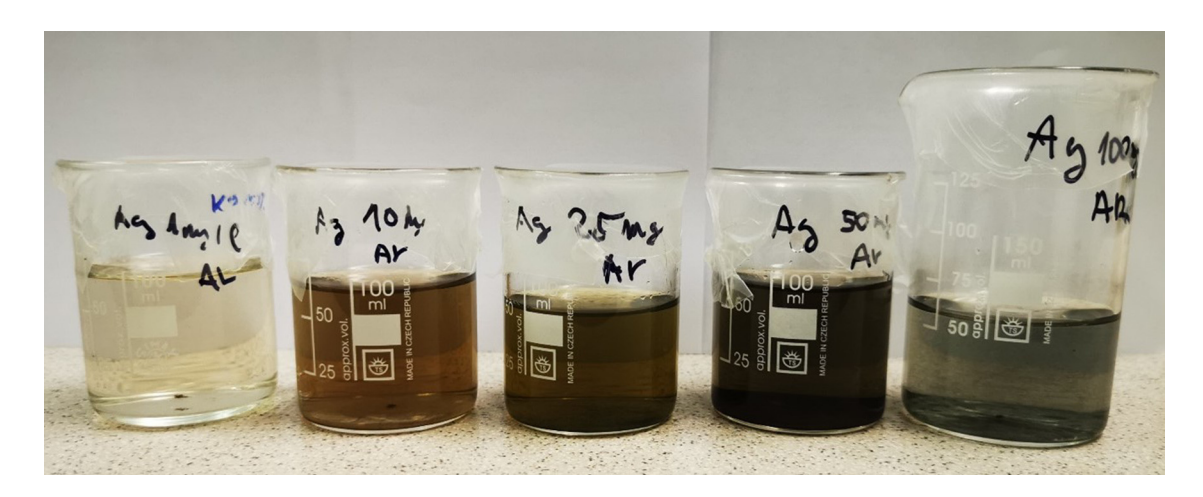


Figure 7: Silver solutions treated with argon flow (after 40 days, mixed).

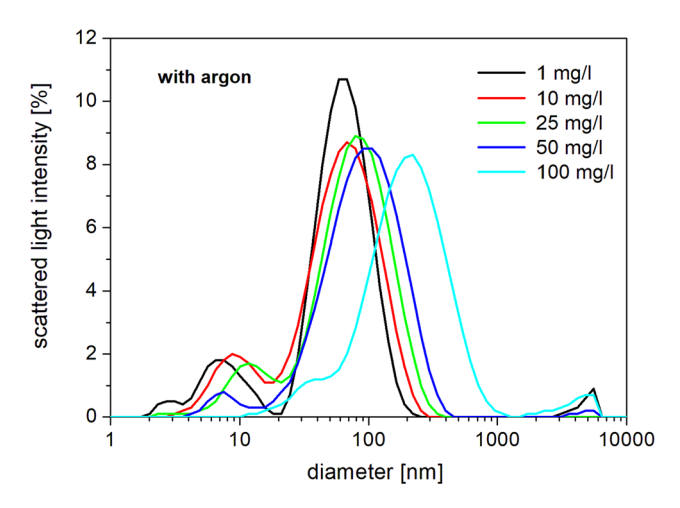


Figure 8: Ag nanoparticle average size distribution for solutions treated with argon.

Thanks to its surface composition, the prepared Ag nanoparticles are considered to be semiconducting [45–47]. Thus, the Tauc diagrams based on the UV/Vis spectra were constructed to get the value of the direct optical band gap energy. The simplified step-by-step procedure is depicted in the supplementary materials; detailed descriptions can be found in previous studies [36,37,48,49]. The calculated optical gap energies for the prepared Ag nanoparticles are presented in Table 2.

Observed values are in a good agreement with the published results, which are in the range of 1.2–3.4 eV [45,46,50]. The optical band gap values do not exhibit any

Table 2: Optical band gaps of Ag nanoparticles

Concentration [mg/l]	$(\alpha h \nu)^2 [eV^2/cm^2]$		
	Ar	NoAr	
1	2.23	2.16	
10	2.21	2.33	
25	2.34	2.20	
50	2.42	2.29	
100	2.17	2.01	

changes dependent on concentration, and they are similar for both nanoparticles' preparation modes. This indicates that the surface chemical composition and surface properties of the same nanoparticles are independent of the precursor concentration.

3.2 Synthesis of copper nanoparticles

Copper nanoparticles were synthetized by the same approach as in the silver nanoparticle case. The 3 min treated solutions were analysed immediately by the UV/Vis spectrometry (Figure 11).

The broader absorption peaks were measured with maximum absorbance close to 300 nm. This reflects that the size of the prepared copper nanoparticles is bigger than in case of Ag nanoparticles as it is confirmed also by the DLS analysis (Table 3 and Figure 12). The samples

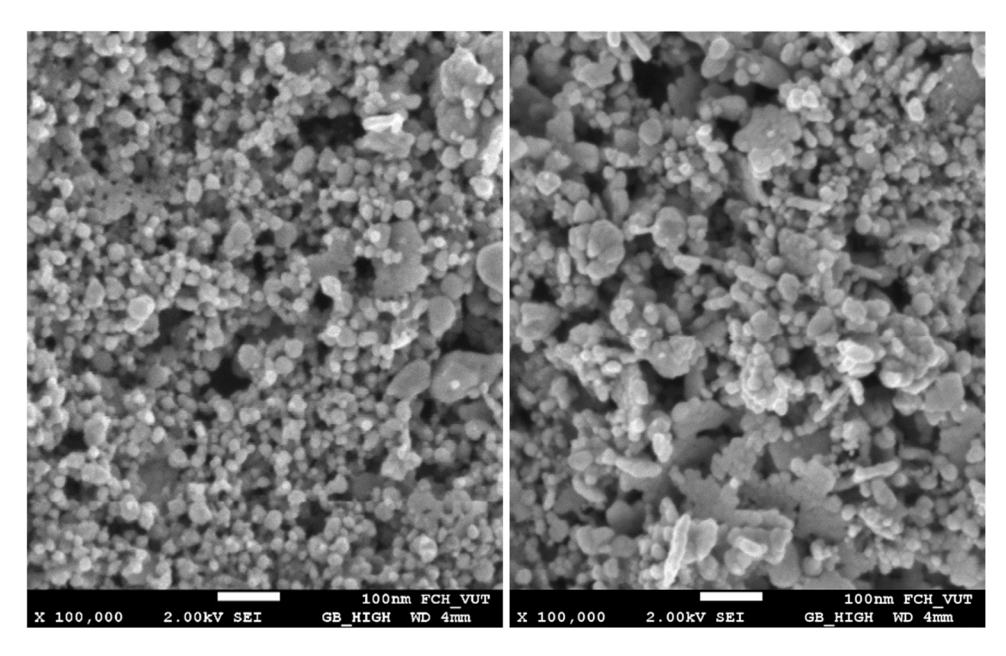


Figure 9: Ag nanoparticles prepared in 100 mg/l solution with (left) and without (right) argon flow.

8 — Jakub Horák *et al.* DE GRUYTER

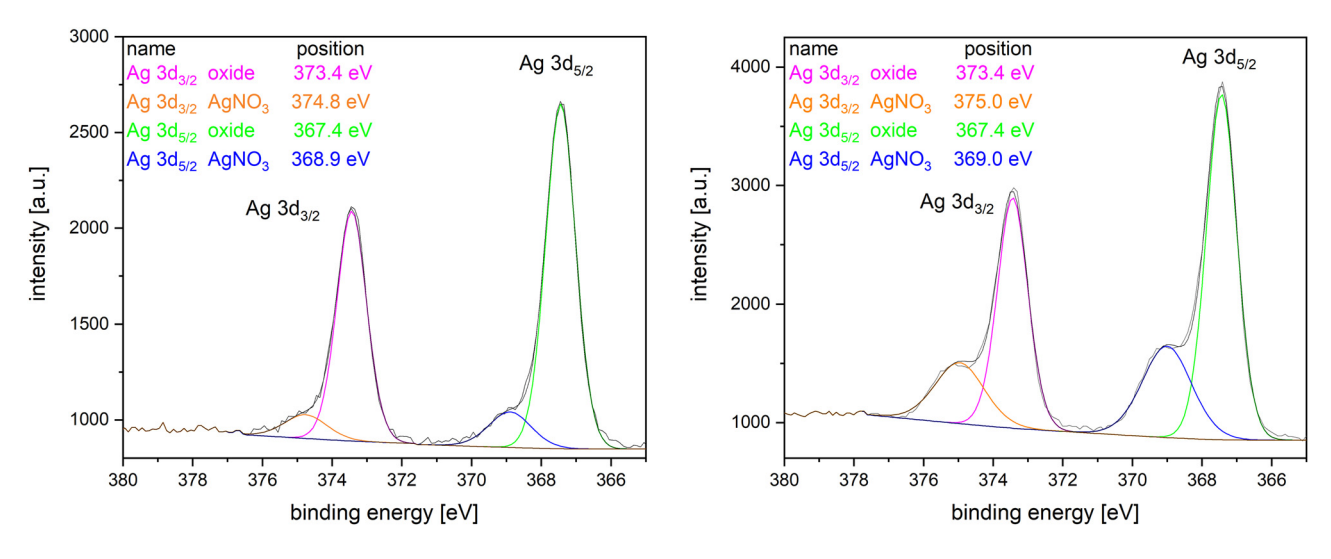


Figure 10: XPS data for Ag particles synthesized with (left) and without (right) argon flow.

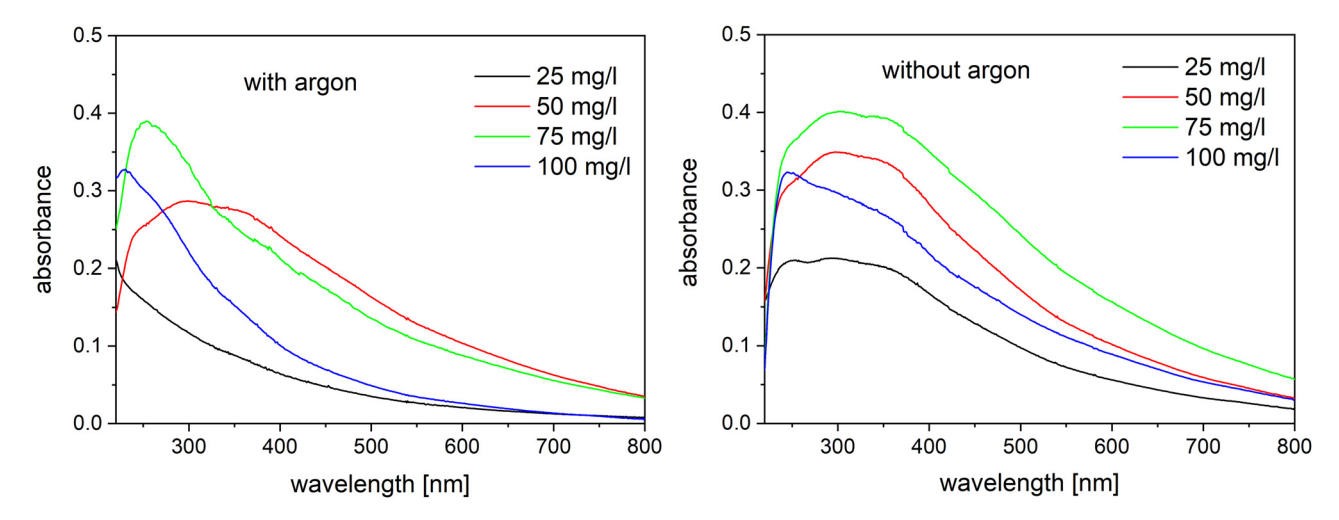


Figure 11: Absorption spectra of the treated copper solutions with (left) and without (right) argon flow.

were filtered with a $0.45\,\mu m$ filter to remove the biggest agglomerates prior to the DLS analysis.

According to the DLS results, argon presence in the discharge leads to the bigger particles formation. The SEM analysis has showed that Cu nanoparticles are nanowhiskers in shape (Figure 13); therefore, DLS analysis for

Table 3: Average diameter results of the DLS analysis for the prepared Cu nanoparticles

		Concentration (mg/l)		
		50	75	100
Average diameter (nm)	Ar NoAr	310 ± 20 240 ± 30	290 ± 70 200 ± 60	240 ± 10 260 ± 30

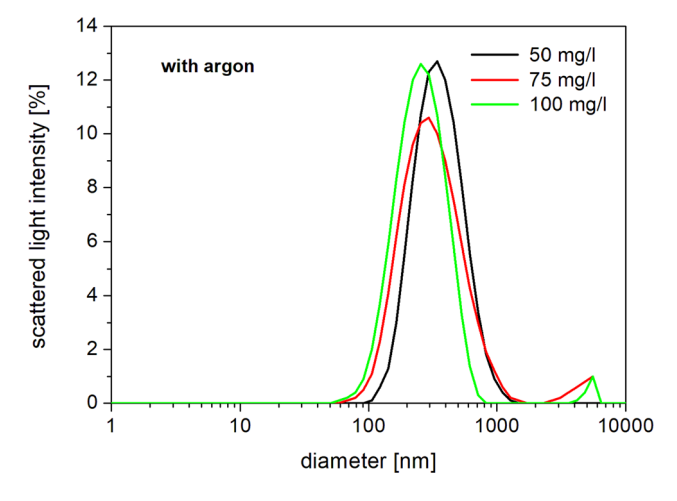


Figure 12: Cu nanoparticle average size distribution for solutions treated with argon.

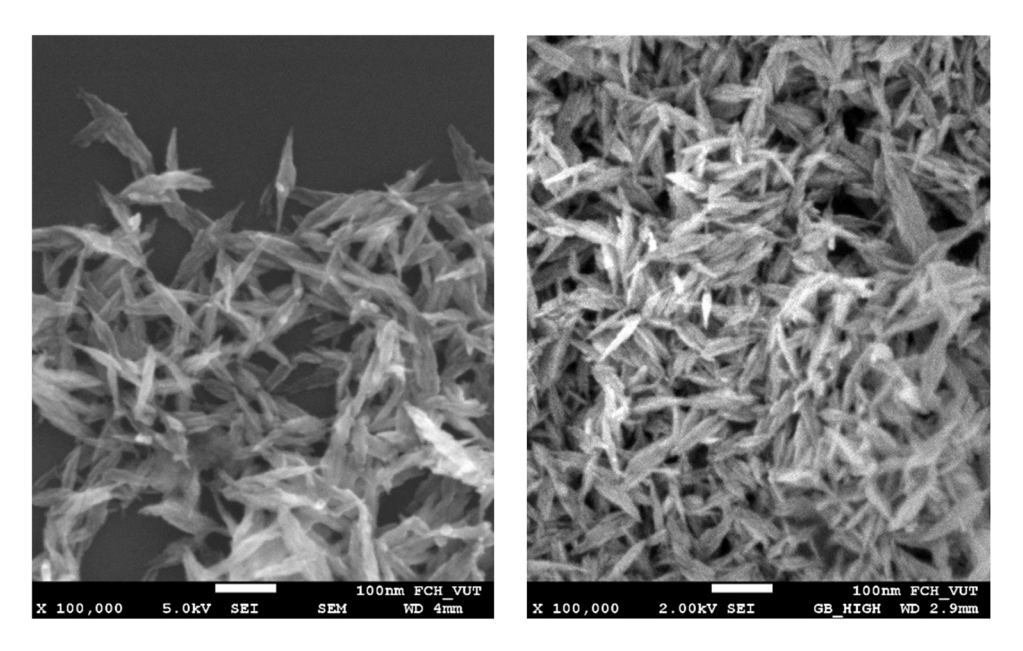


Figure 13: Cu nanoparticles prepared in 75 mg/l solution with (left) and without (right) argon flow.

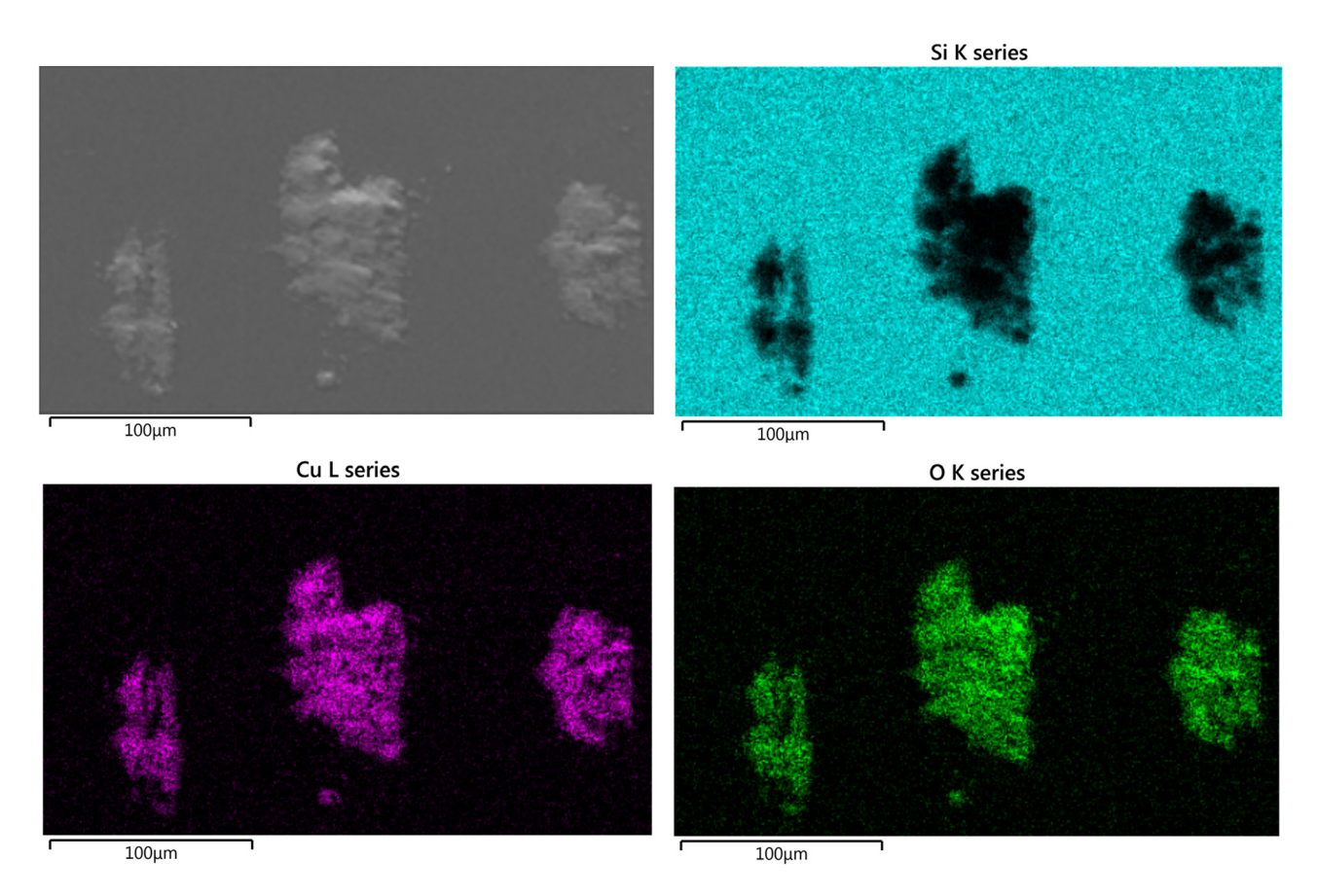


Figure 14: SEM and EDS images of Cu particles.

10 — Jakub Horák et al. DE GRUYTER

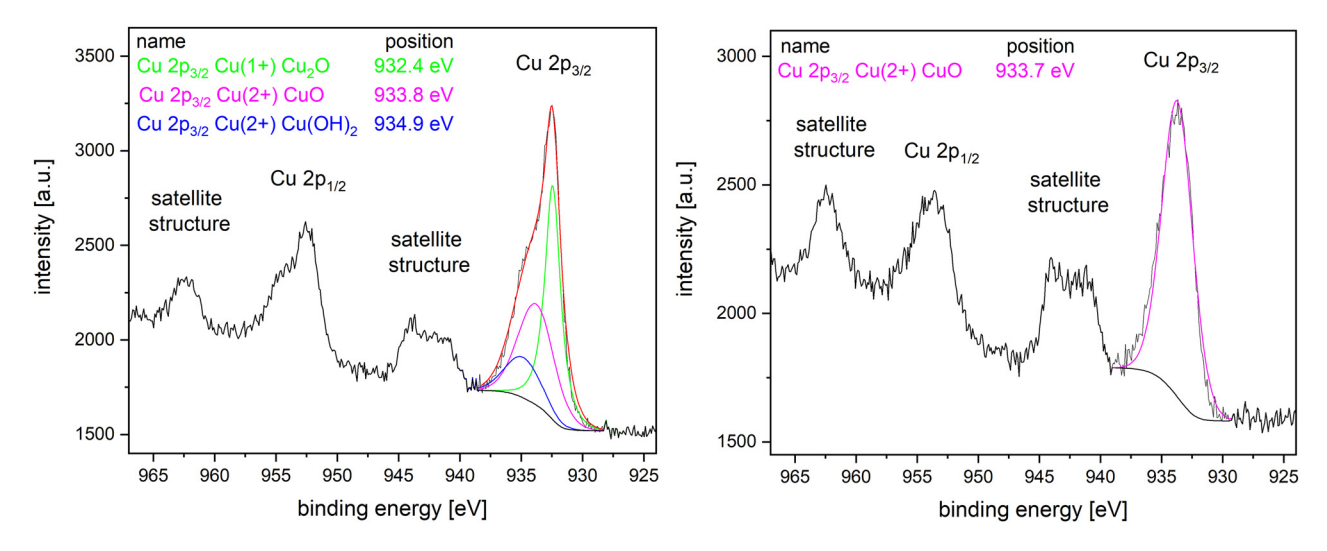


Figure 15: XPS data for Cu particles synthesized with (left) and without (right) argon flow.

Table 4: Optical band gaps of Cu nanoparticles

Concentration [mg/l]	$(\alpha h \nu)^2 [eV^2/cm^2]$		
	Ar	NoAr	
50	2.77	2.68	
75	2.64	2.58	
100	3.77	2.42	

Cu nanoparticles can be used only for a relative comparison between the prepared Cu nanoparticles. The similar structure for the oxidized Cu nanoparticles was observed in the previous studies, too [51,52]. Determined nanoparticles exhibit the length of about 100–150 nm, and as well as in the silver nanoparticles case, they form big agglomerates during the drying step before the SEM imaging.

The non-oxidized Cu⁰ nanoparticles have their absorption peak at about 560–580 nm [53]. No such peak is visible in Figure 11. Thus, it can be assumed that Cu oxide/hydroxide nanoparticles were prepared [54]. To confirm this hypothesis, the EDS (Figure 14) and XPS measurements (Figure 15) were performed.

The EDS element maps (Figure 14) clearly demonstrate that copper nanoparticles are not pure metallic and as can be seen from Figure 15, the copper XPS peak for nanoparticles synthesized with argon contains three sub-peaks; the peak at 932.4 eV for metallic copper/copper(i) oxide, the 933.8 eV peak for the copper oxide, and the 934.9 eV peak for the copper hydroxide while particles synthesized without argon show only copper oxide. Thus, the oxide or hydroxide nanoparticle coverage is confirmed. Compared to silver, no residual signal from the inorganic salt was detected for both cathode configurations. Peak at 932.4 eV could belong to Cu(0) or Cu(1+) as

their binding energies are very close to each other. Normally, they can be distinguished by the measurement of the Auger parameter [55,56], but this is not applicable in our case because of a strong effect of Cu(2+) presence. The calculated Auger parameter is 1850.2 eV, which is just in between the values for Cu(1+) (1848.6–1849.6 eV) and Cu(0) (1850.7–1851.4 eV) [57]. Therefore, we assume that there might be both Cu states, with a possible effect of gradual oxidation over time.

As the presence of oxides and hydroxides at the surface has been confirmed, the nanoparticle characteristics is considered to be semiconductive [58–60]. Thus, the Tauc diagrams based on the UV/Vis spectra were constructed to get the value of the direct optical band gap energy. The calculated optical gap energies for the prepared Cu nanoparticles are presented in Table 4.

Observed values are in a good agreement with the published results, which are in the range of 2.0–2.85 eV [61,62]. The optical band gap values are slightly decreasing with the precursor concentration, and they are similar for both preparation modes of nanoparticles. This indicates the surface chemical composition and surface properties of the same nanoparticles are independent of the precursor concentration. The value obtained at the highest precursor concentration with the argon addition is deviating from other values probably because of the effect of agglomerates formed at such conditions.

4 Conclusion

A new single-step approach in the nanoparticle synthesis directly in the liquid has been demonstrated. The underwater

discharge generated in gaseous bubbles was used for Ag and Cu nanoparticle generation from inorganic salt precursors. Two principal schemes of the reactor with and without argon gas flow were tested and compared in the performance. It was shown that high yield of nanoparticles can be achieved even

without the application of the gas flow.

DE GRUYTER

Formed silver nanoparticles had the spherical-like shape with the size varying in the range of 10–80 nm. The particle size distribution can be controlled by the concentration of the inorganic salt. The increase in the salt concentration results in large particle formation and dependence was stronger in case of the discharge generated in argon bubbles. Chemical composition of Ag nanoparticles was mainly metallic silver covered by the thin silver oxide layer that was confirmed by the XPS analysis and by the band gap calculation. It has been found that the band gap has no dependence on the precursor concentration.

Cu nanoparticles synthesized in both regimes of operation had the nanowhisker shape with the length of about 100–150 nm. In contrast to Ag particles, the latter are tending to fast agglomeration, especially when argon flow is applied through the HV electrode. The chemical composition of Cu nanoparticles is represented by copper oxide/copper hydroxide with the band gap of about 2.4–2.8 eV.

The advantage of the approach presented here is a very high rate of synthesis with no need of any reducing or stabilizing agents. It was revealed that nanoparticles can be synthesized directly in liquid with good short-term stability of days without any stabilizer. The generated Ag nanoparticles in the argon discharge formed a colloidal solution with stability and no agglomeration during weeks. In case of copper nanoparticles, faster agglomeration into bigger clusters was observed probably because of complex shape of the particles. The change of the argon flow should lead to the nanoparticle size tuning, and this may ultimately reduce the consumption of chemicals needed for the nanoparticle preparation. The as-prepared nanoparticles can be used in biomedical area owing to their antibacterial activity, and also, they can be applied for targeted treatment applications using the different surface plasmon resonance.

Acknowledgments: The authors acknowledge the support of the ERASMUS+ program.

Funding information: This work received financial support from the ERASMUS+ program.

Author contributions: All authors have accepted responsibility for the entire content of this manuscript and approved its submission.

Conflict of interest: The authors state no conflict of interest.

References

- [1] Ojha NK, Zyryanov GV, Majee A, Charushin VN, Chupakhin ON, Santra S. Copper nanoparticles as inexpensive and efficient catalyst: A valuable contribution in organic synthesis. Coord Chem Rev. 2017;353:1–57. [cited 2022 Jul 10] doi: 10.1016/j.ccr.2017.10.004.
- [2] Khan FU, Chen Y, Khan NU, Khan ZUH, Khan AU, Ahmad A, et al. Antioxidant and catalytic applications of silver nanoparticles using *Dimocarpus longan* seed extract as a reducing and stabilizing agent. J Photochem Photobiol B. 2016;164:344–51. [cited 2022 Jul 10] doi: 10.1016/j.jphotobiol.2016.09.042.
- [3] Burduşel A-C, Gherasim O, Grumezescu AM, Mogoantă L, Ficai A, Andronescu E. Biomedical applications of silver nanoparticles: An up-to-date overview. Nanomaterials (Basel). 2018;8(9):681. [cited 2022 Jul 10] doi: 10.3390/nano8090681.
- [4] Hemmati S, Ahany Kamangar S, Ahmeda A, Zangeneh MM, Zangeneh A. Application of copper nanoparticles containing natural compounds in the treatment of bacterial and fungal diseases. Appl Organomet Chem. 2020;34(4):e5465. [cited 2022 Jul 10] doi: 10.1002/aoc.5465.
- [5] Lu Z, Rong K, Li J, Yang H, Chen R. Size-dependent antibacterial activities of silver nanoparticles against oral anaerobic pathogenic bacteria. J Mater Sci: Mater Med. 2013;24(6):1465–71. [cited 2022 Aug 10] doi: 10.1007/s10856-013-4894-5.
- [6] Zhang M, Zhao F, Li H, Yang Y, An T, Jiang Y, et al. Morphology-dependent catalytic activity of Fe₂O₃ and its graphene-based nanocomposites on the thermal decomposition of AP. FirePhysChem. 2021;1(1):46–53. [cited 2022 Aug 10] doi: 10.1016/j. fpc.2021.02.002.
- [7] Kanade P, Yadav P, Kumar M, Tripathi B. Plasmon-induced photon manipulation by Ag nanoparticle-coupled graphene thin-film: Light trapping for photovoltaics. Plasmonics. 2015;10(1):157–64. [cited 2022 Aug 10] doi: 10.1007/s11468-014-9790-4.
- [8] Mo L, Guo Z, Wang Z, Yang L, Fang Y, Xin Z, et al. Nano-silver ink of high conductivity and low sintering temperature for paper electronics. Nanoscale Res Lett. 2019;14(1):197. [cited 2022 Aug 10] doi: 10.1186/s11671-019-3011-1.
- [9] Kokura S, Handa O, Takagi T, Ishikawa T, Naito Y, Yoshikawa T. Silver nanoparticles as a safe preservative for use in cosmetics. Nanomedicine. 2010;6(4):570–4. [cited 2022 Aug 10] doi: 10.1016/j. nano.2009.12.002.
- [10] Fytianos G, Rahdar A, Kyzas GZ. Nanomaterials in cosmetics: Recent updates. Nanomaterials (Basel). 2020;10(5):979. [cited 2022 Aug 10] doi: 10.3390/nano10050979.
- [11] Li W, Sun Q, Li L, Jiu J, Liu X-Y, Kanehara M, et al. The rise of conductive copper inks: Challenges and perspectives. Appl Mater Today. 2020;18:100451. [cited 2022 Jul 10] doi: 10.1016/j.apmt.2019. 100451
- [12] Gawande MB, Goswami A, Felpin F-X, Asefa T, Huang X, Silva R, et al. Cu and Cu-based nanoparticles: Synthesis and applications in catalysis. Chem Rev. 2016;116(6):3722–811. [cited 2022 Aug 10] doi: 10.1021/acs.chemrev.5b00482.
- [13] Zamani A, Poursattar Marjani A, Nikoo A, Heidarpour M, Dehghan A. Synthesis and characterization of copper nanoparticles on walnut shell for catalytic reduction and C-C coupling reaction.

- Inorg Nano-Met Chem. 2018;48(3):176-81. [cited 2022 Aug 10] doi: 10.1080/24701556.2018.1503676.
- [14] Paszkiewicz M, Gołąbiewska A, Rajski Ł, Kowal E, Sajdak A, Zaleska-Medynska A. Synthesis and characterization of monometallic (Ag, Cu) and bimetallic Ag-Cu particles for antibacterial and antifungal applications. J Nanomater. 2016;2016:1-11. [cited 2022 Jul 10] doi: 10.1155/2016/2187940.
- [15] Zia R, Riaz M, Faroog N, Qamar A, Anjum S. Antibacterial activity of Ag and Cu nanoparticles synthesized by chemical reduction method: A comparative analysis. Mater Res Express. 2018;5(7):075012. [cited 2022 Jul 10] doi: 10.1088/2053-1591/aacf70.
- [16] Mahmoodi S, Elmi A, Hallaj Nezhadi S. Copper nanoparticles as antibacterial agents. J Mol Pharm Org Process Res. 2018;6(1):1000140. [cited 2022 Aug 10] doi: 10.4172/2329-9053.1000140.
- [17] Abou El-Nour KMM, Eftaiha A, Al-Warthan A, Ammar RAA. Synthesis and applications of silver nanoparticles. Arab J Chem. 2010;3(3):135-40. [cited 2022 Aug 10] doi: 10.1016/j.arabjc.2010. 04.008.
- [18] Bhaskar D, Sanjukta P. Antimicrobials: Meeting the challenges of antibiotic resistance through nanotechnology. In: Nanostructures for antimicrobial therapy. Netherlands: Elsevier; 2017. p. 1-22.
- [19] El-Saadony MT, Abd El-Hack ME, Taha AE, Fouda MMG, Ajarem JS, Maodaa NS, et al. Ecofriendly synthesis and insecticidal application of copper nanoparticles against the storage pest Tribolium castaneum. Nanomaterials (Basel). 2020;10(3):587. [cited 2022 Aug 10] doi: 10.3390/nano10030587.
- [20] Iravani S, Korbekandi H, Mirmohammadi SV, Zolfaghari B. Synthesis of silver nanoparticles: Chemical, physical and biological methods. Res Pharm Sci. 2014;9(6):385-406.
- [21] Mariotti D, Patel J, Švrček V, Maguire P. Plasma-liquid interactions at atmospheric pressure for nanomaterials synthesis and surface engineering. Plasma Process Polym. 2012;9(11-12):1074-85. [cited 2022 Aug 10] doi: 10.1002/ppap.201200007.
- [22] Mariotti D, Sankaran RM. Microplasmas for nanomaterials synthesis. J Phys D Appl Phys. 2010;43(32):323001. [cited 2022 Aug 10] doi: 10.1088/0022-3727/43/32/323001.
- [23] Rao N, Girshick S, Heberlein J, McMurry P, Jones S, Hansen D, et al. Nanoparticle formation using a plasma expansion process. Plasma Chem Plasma Process. 1995;15(4):581–606. [cited 2022 Aug 10] doi: 10.1007/bf01447062.
- [24] Chang F-C, Richmonds C, Sankaran RM. Microplasma-assisted growth of colloidal Ag nanoparticles for point-of-use surfaceenhanced Raman scattering applications. J Vac Sci Technol A. 2010;28(4):L5-8. [cited 2022 Aug 10] doi: 10.1116/1.3428708.
- [25] Rumbach P, Witzke M, Sankaran RM, Go DB. Plasma-liquid interactions: Separating electrolytic reactions from plasma/gas phase reactions. In: Proceedings of the 2013 ESA Annual Meeting on Electrostatics; 2013. p. 1-8. on Electrostatics.
- [26] Richmonds C, Sankaran RM. Plasma-liquid electrochemistry: Rapid synthesis of colloidal metal nanoparticles by microplasma reduction of aqueous cations. Appl Phys Lett. 2008;93(13):131501. [cited 2022 Aug 10]. doi: 10.1063/1.2988283.
- [27] Jabłońska J, Jankowski K, Tomasik M, Cykalewicz D, Uznański P, Całuch S, et al. Preparation of silver nanoparticles in a high voltage AC arc in water. SN Appl Sci. 2021;3(2). [cited 2022 Jul 10]. doi: 10.1007/s42452-021-04177-4.
- [28] Muto H, Miyajima K, Mafuné F. Mechanism of laser-induced size reduction of gold nanoparticles as studied by single and double laser pulse excitation. J Phys Chem C Nanomater Interfaces. 2008;112(15):5810-5. [cited 2022 Aug 10] doi: 10.1021/jp711353m.

- [29] Barmina EV, Gudkov SV, Simakin AV, Shafeev GA. Stable products of laser-induced breakdown of aqueous colloidal solutions of nanoparticles. J Laser Micro/Nanoeng. 2017;12(3):254-7. [cited 2022 Jul 10] doi: 10.2961/jlmn.2017.03.0014.
- [30] Khezri SH, Yazdani A, Khordad R, Ravan BA. Preparation of pure cobalt nanoparticles by electric arc discharge method in ethylene glycol. Mod Phys Lett B. 2013;27(9):1350057. [cited 2022 Aug 10] doi: 10.1142/s0217984913500577.
- [31] Čechová L, Krčma F, Kalina M, Man O, Kozáková Z. Preparation of silver and gold nanoparticles by the pinhole DC plasma system. J Appl Phys. 2021;129(23):233304. [cited 2022 Jul 10] doi: 10.1063/5. 0044054.
- [32] Krčma F. Method for plasma generation in liquids using a jet system. European Patent. 3122161B1: 2019.
- [33] Krcma F, Klimova E, Mazankova V, Dostal L, Obradovic B, Nikiforov A, et al. Novel plasma source based on pin-hole discharge configuration. Plasma Med. 2016;6(1):21–31. [cited 2022 Jul 10] doi: 10.1615/plasmamed.2016015850.
- [34] Krčma F. Nozzle system for generating plasma in bubbles in liquids. Util Model. 2016;30097.
- [35] Krčma F, Kozáková Z, Mazánková V, Horák J, Dostál L, Obradović B, et al. Characterization of novel pin-hole based plasma source for generation of discharge in liquids supplied by DC non-pulsing voltage. Plasma Sources Sci Technol. 2018;27(6):065001. [cited 2022 Jul 10] doi: 10.1088/1361-6595/aac521.
- [36] Makuła P, Pacia M, Macyk W. How to correctly determine the band gap energy of modified semiconductor photocatalysts based on UV-Vis spectra. J Phys Chem Lett. 2018;9(23):6814-7. [cited 2022 Aug 11] doi: 10.1021/acs.jpclett.8b02892.
- [37] Jubu PR, Yam FK, Igba VM, Beh KP. Tauc-plot scale and extrapolation effect on bandgap estimation from UV-vis-NIR data - A case study of β-Ga₂O₃. J Solid State Chem. 2020;290:121576. [cited 2022 Jul 10] doi: 10.1016/j.jssc.2020.121576.
- [38] Lukes P, Clupek M, Babicky V, Spetlikova E, Sisrova I, Marsalkova E, et al. High power DC diaphragm discharge excited in a vapor bubble for the treatment of water. Plasma Chem Plasma Process. 2013;33(1):83-95. [cited 2022 Aug 11] doi: 10.1007/s11090-012-
- [39] Kozáková Z, Krčma F, Čechová L, Simic S, Doskočil L. Generation of silver nanoparticles by the pin-hole DC plasma source with and without gas bubbling. Plasma Phys Technol J. 2019;6(2):180-3. [cited 2022 Dec 15] doi: 10.14311/ppt.2019.2.180.
- [40] Acharya TR, Lee GJ, Choi EH. Influences of plasma plume length on structural, optical and dye degradation properties of citrate-stabilized silver nanoparticles synthesized by plasma-assisted reduction. Nanomaterials (Basel). 2022;12(14):2367. [cited 2022 Dec 15] doi: 10.3390/nano12142367.
- [41] Kozáková Z, Nejezchleb M, Krčma F, Halamová I, Čáslavský J, Dolinová J. Removal of organic dye Direct Red 79 from water solutions by DC diaphragm discharge: Analysis of decomposition products. Desalination. 2010;258(1-3):93-9. [cited 2022 Dec 15] doi: 10.1016/j.desal.2010.03.038.
- [42] Yan B, Zhou H, Gardea-Torresdey JL, editors. Bioactivity of engineered nanoparticles. 1st edn. Singapore, Singapore: Springer; 2017.
- [43] Jorge de Souza TA, Rosa Souza LR, Franchi LP. Silver nanoparticles: An integrated view of green synthesis methods, transformation in the environment, and toxicity. Ecotoxicol Environ Saf. 2019;171:691-700. [cited 2022 Dec 15] doi: 10.1016/j.ecoenv.2018. 12.095.

DE GRUYTER

- [44] Rajesh KM, Ajitha B, Ashok Kumar Reddy Y, Suneetha Y, Sreedhara Reddy P. Synthesis of copper nanoparticles and role of pH on particle size control. Mater Today. 2016;3(6):1985-91. [cited 2022 Dec 15] doi: 10.1016/j.matpr.2016.04.100.
- [45] Salim ET, Awayiz MT. Silver oxide nanostructure: A study on physical properties at different chemical interaction time. Res Sq. 2021. [cited 2022 Dec 15] doi: 10.21203/rs.3.rs-249392/v1.
- [46] Widyaningtyas AL, Yulizar Y, Bagus Apriandanu DO. Ag₂O nanoparticles fabrication by Vernonia amygdalina Del. leaf extract: synthesis, characterization, and its photocatalytic activities. IOP Conf Ser Mater Sci Eng. 2019;509:012022. [cited 2022 Dec 15] doi: 10.1088/1757-899x/509/1/012022.
- [47] Jeung D-G, Lee M, Paek S-M, Oh J-M. Controlled growth of silver oxide nanoparticles on the surface of citrate anion intercalated layered double hydroxide. Nanomaterials (Basel). 2021;11(2):455. [cited 2022 Dec 15] doi: 10.3390/nano11020455.
- [48] Dhineshbabu NR, Rajendran V, Nithyavathy N, Vetumperumal R. Study of structural and optical properties of cupric oxide nanoparticles. Appl Nanosci. 2016;6(6):933-9. [cited 2022 Aug 11] doi: 10. 1007/s13204-015-0499-2.
- [49] Raciti R, Bahariqushchi R, Summonte C, Aydinli A, Terrasi A, Mirabella S. Optical bandgap of semiconductor nanostructures: Methods for experimental data analysis. J Appl Phys. 2017;121(23):234304. [cited 2022 Jul 10] doi: 10.1063/1.4986436.
- [50] Mistry H, Thakor R, Patil C, Trivedi J, Bariya H. Biogenically proficient synthesis and characterization of silver nanoparticles employing marine procured fungi Aspergillus brunneoviolaceus along with their antibacterial and antioxidative potency. Biotechnol Lett. 2021;43(1):307-16. [cited 2022 Dec 15] doi: 10.1007/s10529-020-03008-7.
- [51] Anandan S, Yang S. Emergent methods to synthesize and characterize semiconductor CuO nanoparticles with various morphologies - an overview. | Exp Nanosci. 2007;2(1-2):23-56. [cited 2022 Aug 16] doi: 10.1080/17458080601094421.
- [52] Wang W, Zhan Y, Wang X, Liu Y, Zheng C, Wang G. Synthesis and characterization of CuO nanowhiskers by a novel one-step, solidstate reaction in the presence of a nonionic surfactant. Mater Res Bull. 2002;37(6):1093-100. [cited 2022 Aug 16] doi: 10.1016/s0025-5408(02)00745-6.

- [53] Henglein A. Formation and absorption spectrum of copper nanoparticles from the radiolytic reduction of Cu(CN)₂-. J Phys Chem B. 2000;104(6):1206-11. [cited 2022 Jul 10] doi: 10.1021/jp992950q.
- [54] Renuga D, Jeyasundari J, Shakthi Athithan AS, Brightson Arul Jacob Y. Synthesis and characterization of copper oxide nanoparticles using Brassica oleracea var. italic extract for its antifungal application. Mater Res Express. 2020;7(4):045007. [cited 2022 Jul 10] doi: 10.1088/2053-1591/ab7b94.
- [55] Ghodselahi T, Vesaghi MA, Shafiekhani A, Baghizadeh A, Lameii M. XPS study of the Cu@Cu2O core-shell nanoparticles. Appl Surf Sci. 2008;255(5):2730-4. [cited 2022 Dec 15] doi: 10.1016/j.apsusc.2008.08.110.
- [56] Biesinger MC. Advanced analysis of copper X-ray photoelectron spectra: Advanced analysis of copper X-ray photoelectron spectra. Surf Interface Anal. 2017;49(13):1325-34. [cited 2022 Dec 15] doi: 10. 1002/sia 6239
- [57] NIST X-ray Photoelectron Spectroscopy Database, NIST Standard Reference Database Number 20, National Institute of Standards and Technology, Gaithersburg MD, 20899 (2000). 10.18434/T4T88K. (retrieved [2022 Dec 15]).
- [58] Zoolfakar AS, Rani RA, Morfa AJ, O'Mullane AP, Kalantar-zadeh K. Nanostructured copper oxide semiconductors: A perspective on materials, synthesis methods and applications. J Mater Chem C Mater Opt Electron Devices. 2014;2(27):5247-70. [cited 2022 Jul 10] doi: 10.1039/c4tc00345d.
- [59] Rahnama A, Gharagozlou M. Preparation and properties of semiconductor CuO nanoparticles via a simple precipitation method at different reaction temperatures. Opt Quantum Electron. 2012;44(6-7):313-22. [cited 2022 Jul 10] doi: 10.1007/s11082-011-9540-1.
- Song X, Sun S, Zhang W, Yu H, Fan W. Synthesis of Cu(OH)₂ nanowires at aqueous-organic interfaces. J Phys Chem B. 2004;108(17):5200-5. [cited 2022 Jul 10] doi: 10.1021/jp036270w.
- Murali DS, Kumar S, Choudhary RJ, Wadikar AD, Jain MK, Subrahmanyam A. Synthesis of Cu₂O from CuO thin films: Optical and electrical properties. AIP Adv. 2015;5(4):047143. [cited 2022 Aug 16] doi: 10.1063/1.4919323.
- [62] Sagadevan S, Pal K, Chowdhury ZZ. Fabrication of CuO nanoparticles for structural, optical and dielectric analysis using chemical precipitation method. J Mater Sci: Mater Electron. 2017;28(17):12591-7. [cited 2022 Aug 17] doi: 10.1007/s10854-017-7083-3.